

## A MULTIREOLUTION INFRARED IMAGING STUDY OF LkH $\alpha$ 198

CHRIS D. KORESKO<sup>1</sup> AND PAUL M. HARVEY

McDonald Observatory, RLM 16.228, University of Texas, Austin, TX 78712-1083

JULIAN C. CHRISTOU AND ROBERT Q. FUGATE

Starfire Optical Range, Kirtland AFB, NM 87117-5776

AND

WENBIN LI

McDonald Observatory, RLM 16.228, University of Texas, Austin, TX 78712-1083

Received 1996 December 16; accepted 1997 March 17

### ABSTRACT

New near-infrared images of the young, nebulous, intermediate-mass (Herbig Ae/Be) star LkH $\alpha$  198 using direct imaging, adaptive-optics compensated speckle imaging, and standard speckle imaging reveal complex structure in its circumstellar dust distribution. At high resolution, LkH $\alpha$  198 is found to possess a barlike feature which extends  $\sim 3''$  from the star in either direction. Geometrical considerations suggest that the bar is unlikely to represent light scattered by either a standard circumstellar disk, a disequilibrium “pseudodisk,” or an ambient halo illuminated by starlight escaping along the polar axis of a disk. Its orientation suggests that it may be associated with the fan-shaped nebula that surrounds LkH $\alpha$  198. The infrared companion  $6''$  north of the star is found to be significantly extended at near-infrared wavelengths and may be an example of a deeply embedded object with an envelope that is at least partially illuminated from the outside.

*Subject headings:* circumstellar matter — ISM: individual (LkH 198) — stars: pre-main sequence — techniques: interferometric

### 1. INTRODUCTION

The Herbig Ae/Be stars are intermediate-mass pre-main sequence stars that exhibit emission lines and are associated with nebulosity (Herbig 1960). They are often regarded as intermediate-mass analogs of the low-mass T Tauri (TTS) class of pre-main sequence stars. Like the TTS, the Herbig Ae/Be stars are often found to possess extended halos on subarcsecond and larger scales (e.g., Leinert, Haas, & Weitzel 1993; Kataza & Maihara 1991; Li et al. 1994) and large infrared excesses that have been interpreted as the signatures of optically thick circumstellar disks (Hillenbrand et al. 1992). However, the nature of the dust distributions surrounding the Ae/Be stars is still very much in question. It is clear that disks alone cannot account for all of their observed properties. For example, several Ae/Be stars have been found to be much more extended at far-infrared wavelengths than the pure star + disk model would predict (Natta et al. 1993; Di Francesco et al. 1994). Spherically symmetric halo models can reproduce their spectral energy distributions, but disks may still be present at smaller linear scales (Natta et al. 1993).

Near-infrared (NIR) images taken over a range of angular resolutions are a useful means for studying the Ae/Be stars. Seeing-limited direct images can be used to probe extended, relatively faint structure on scales appropriate for examining the overall interaction between the stars and their surrounding cloud material. Adaptive-optics (AO) and speckle observations can resolve the bright light scattered by circumstellar dust on scales of hundreds to thousands of AU, where the light distribution is less likely to be confused by the more extended nebulosity associated

with the ambient cloud. These images may give clues to the presence of optically thick material closer to the star. For example, a bipolar nebula may be used to infer the presence of a disk.

LkH $\alpha$  198 is a Herbig Ae/Be star in a small dark cloud at a distance of some 600–900 pc (Herbig 1960; Chavarria 1985). The region has attracted considerable attention in recent years, resulting in the discovery of a number of Herbig-Haro (HH) objects tracing at least two jets (Strom et al. 1986; Corcoran, Ray, & Bastien 1995, hereafter CRB), an infrared-bright embedded companion (Lagage et al. 1993), and a submillimeter continuum peak that has been interpreted as a protostar (Sandell & Weintraub 1994). Both stars, the protostar, and V376 Cas, a second Herbig Ae/Be star  $35''$  north of LkH $\alpha$  198, have variously been proposed as the driving source for a low-velocity bipolar molecular outflow detected in CO (Loren 1977; Cantó et al. 1984; Chavarria 1985; Nakano et al. 1990).

### 2. OBSERVATIONS

Previous visible-light and infrared observations of LkH $\alpha$  198 have revealed a complex distribution of matter with structure over a wide range of linear scales. We have applied three complementary observational techniques to examine these systems with resolutions between  $0''.35$  and  $1''.3$  and fields of view from  $10''$ – $100''$ . Direct imaging is limited to the seeing resolution, which is approximately an order of magnitude poorer than the diffraction limit, but it offers high flux sensitivity. AO compensated speckle observations made with a telescope of modest aperture permit higher resolution but with lower sensitivity than direct images. Speckle interferometry with a larger, passive optical system gives a small field of view and poor sensitivity to faint extended structure but can produce very high resolution if the source is sufficiently bright.

<sup>1</sup> Current address: Division of Geological and Planetary Sciences, California Institute of Technology, Pasadena, CA 91125.

### 2.1. Direct Infrared Imaging

Infrared images of the region surrounding LkH $\alpha$  198 were taken in the *J* (1.25  $\mu\text{m}$ ), *H* (1.65  $\mu\text{m}$ ), and *K* (2.2  $\mu\text{m}$ ) photometric bands with the Rokcam infrared camera at the Cassegrain focus of the 2.7 m Harlan J. Smith telescope at the McDonald Observatory on 1993 November 21. These images have been published previously in Li et al. (1994). The camera is based on a NICMOS-3 HgCdTe detector with an array of  $256 \times 256$  pixels with a spacing of  $0''.40$ , giving a field of  $1''.7$ . The seeing was fairly good ( $1''.3$ ), but thin cirrus precluded absolute photometry.

Integrations on the science target consisted of series of 10 or 20 frames with 0.5–5.0 s exposure time each. Similar observations were made of the unresolved star HD 203856, providing crude estimates of the point-spread function (PSF) (Table 1). A dark frame was subtracted from each raw frame, and the results were co-added and divided by flat-field frames to correct for variations in sensitivity between pixels. Bad pixels were “fixed” by spline interpolation. Residual imperfections due to the sky and telescope background could be seen in the corners of the frames, but comparison with frames taken on other objects at the same wavelengths and integration times demonstrated that these imperfections were too small to impact the interpretation of the data.

### 2.2. Adaptive-Optics Compensated Speckle Imaging

Observations of LkH $\alpha$  198 in the 1.65  $\mu\text{m}$  photometric *H* band were conducted at the 1.5 m telescope at the Starfire Optical Range on 1995 October 25. The telescope is equipped with a high-performance AO system designed primarily to operate at visual wavelengths (Fugate et al. 1994). The system is based on a 241 actuator deformable mirror and two 208 subaperture Shack-Hartmann wavefront sensors employing  $64 \times 64$  pixel silicon CCD arrays. One wavefront sensor is optimized for observing a laser beacon in the 500–600 nm band and the other for observing natural stars in the band from 600–750 nm. The AO loop can be operated from either wavefront sensor. A separate fast steering mirror, controlled by a  $4 \times 4$  array of photon counting avalanche photodiodes, corrects the full aperture wavefront tilt. The beam of a 150 W copper-vapor laser is projected from the full aperture of the 1.5 m telescope and focused at a range of 10.5 km. The Rayleigh backscattered light from a range-gated 2.4 km long focal volume served as the wavefront reference for higher order corrections.

The science instrument was D-LITE, an infrared camera built at the University of Texas and optimized for imaging

at high angular resolution. It is based on a single  $128 \times 128$  pixel quadrant of a NICMOS-3 HgCdTe detector, and is equipped with standard *J*, *H*, and *K* broadband photometric filters with center wavelengths of 1.25, 1.65, and 2.2  $\mu\text{m}$ , respectively. The camera was mounted at the  $f/20$  Coudé focus, producing a  $0''.10$  pixel spacing to approximately Nyquist sample the diffraction limited resolution in the *H* band. The overall quantum efficiency of the system, measured as the number of photoelectrons produced in the detector per source photon incident on the atmosphere, was approximately 11%.

Because the laser beam’s return path through the atmosphere was identical to its outbound path, the “laser guidestar” appeared stationary at the telescope focus and could not be used to measure the wavefront tilt. The science objects themselves were too faint for this purpose, and no natural guide stars of adequate brightness lay within the isokinetic area. This necessitated a compromise observing technique in which speckle interferometric procedures were used to correct for the image motion and for any residual high-order wavefront errors. We refer to this technique as Adaptive-Optics Compensated Speckle Imaging (AOCSI). The image, which was presumably nearly diffraction-limited but with significant uncorrected seeing motion, was sampled with series of 400 frames of 0.1 s each, short enough to approximately “freeze” the image. Each series of frames on LkH $\alpha$  198 (the “object”) was immediately preceded or followed by a series on SAO 21077, a nearby star of similar infrared brightness, which served as a point-source reference. Four such object + reference pairs were taken. Two series of 100 frames on blank sky served to measure the background pixel level and Fourier power spectrum. Observations of known binary stars were used to measure the pixel scale and image orientation.

In order to avoid sporadic bad pixels or other effects, frames were rejected if their minimum, maximum, or summed pixel values exhibited large deviations from the average values of those quantities over the series of frames. In addition, some frames were rejected because of a loss of the AO loop during two of the series, and because of an interaction with the display of the raw frames by the data-acquisition system that caused every 25th frame to have a high zero-flux level. The number of frames remaining in a series after these were eliminated was between 287 and 371.

The remaining raw frames were processed using standard speckle interferometric reduction techniques. For each frame, this involved subtracting an averaged sky frame and “fixing” bad pixels by setting their values equal to the average value of their neighbors. The frames in each series

TABLE 1  
JOURNAL OF OBSERVATIONS

Object	Technique	$\lambda$ ( $\mu\text{m}$ )	Reference Star	$\tau$ (s)	Number	Date	Tel	Camera
Region .....	Direct	1.25	...	5.0	10 frames	1993 Nov 21	2.7 m	Rokcam
Region .....	Direct	1.65	...	2.0	20 frames	1993 Nov 21	2.7 m	Rokcam
Region .....	Direct	2.2	...	0.5	20 frames	1993 Nov 21	2.7 m	Rokcam
HD 203856 .....	Direct	1.25	...	0.5	20 frames	1993 Nov 21	2.7 m	Rokcam
HD 203856 .....	Direct	1.65	...	0.5	20 frames	1993 Nov 21	2.7 m	Rokcam
HD 203856 .....	Direct	2.2	...	0.5	20 frames	1993 Nov 21	2.7 m	Rokcam
LkH $\alpha$ 198 .....	AOCSI	1.65	SAO 21077	0.1	4 pairs	1995 Oct 25	1.5 m	D-LITE
LkH $\alpha$ 198 .....	Speckle	1.65	SAO 21188	0.1	8 pairs	1993 Dec 07	2.7 m	Rokcam

were then transformed into the Fourier domain, and their power spectra and bispectra (Lohmann, Weigelt, & Wirtzner 1983) were averaged. The series were then processed in pairs consisting of one object series and one reference series each. For each object + reference pair, the power spectrum of the blank sky was subtracted from the power spectra of the object and the reference star, and the object power was then divided by the reference power to compensate for the transfer functions of the atmosphere and telescope. Corrupted frequencies in the resulting power spectrum were "fixed" in the same way as for bad pixels. The power spectrum was then apodized to 0".8 resolution full width at half maximum (FWHM) by multiplying it by a function  $A(k)$ , the value of which decreased smoothly from unity at zero frequency to zero at a cutoff frequency of 2 cycles arcsec $^{-1}$ . The cutoff frequency is significantly below the diffraction limit of the telescope because the source was too faint to enable higher frequencies to be measured cleanly. The apodizing function chosen was the product of a Gaussian and a Hanning function:

$$A(k) = \begin{cases} \frac{1}{2} \left( 1 + \cos \frac{\pi k}{\alpha} \right) e^{-\left(\frac{k}{\alpha}\right)^2} & \text{if } k < \alpha \\ 0 & \text{otherwise,} \end{cases}$$

where  $k$  is the magnitude of the spatial frequency and  $\alpha$  is the apodization cutoff.

The Fourier phase was reconstructed from the average bispectrum using the "recursive" method, avoiding the use of frequencies with large power in the sky frames (which might have resulted from pickup noise in the camera electronics) whenever possible. The phase recovered from a reference series was subtracted from the phase from each object series to correct for optical aberrations. A slope was added to the resulting phase from each object series in order to shift the position of the peak in the reconstructed image to match that of the original frames. This was necessary to prevent structure close to the edges of the detector from being wrapped around to the opposite side of the image when the peak was not centered on the detector. The Fourier transform for each object series was constructed from the compensated power and phase and inverted to recover a single-pair image. The single-pair images were then shifted to a common center, rotated to correct for the rotation of the image plane at the Coudé focus, and averaged to form the final image.

### 2.3. Speckle Imaging

Speckle interferometric observations of LkH $\alpha$  198 were conducted in the  $H$  band on 1993 December 7 using the Rokcam camera at the Cassegrain focus of the 2.7 m telescope. A negative lens ahead of the telescope focus was used to produce the 0".07 pixel scale needed to approximately Nyquist sample the diffraction limit. Eight object + reference pairs were taken, each consisting of a series of 500 frames of 0.1 s each on the target and 500 on a nearby SAO star. These object + reference pairs were interspersed with measurements of blank sky. The data reduction techniques were similar to those described above for the AOCSI observations, except that no derotation of the images was needed, and the final image was produced by inverting the average of the single-pair Fourier transforms instead of averaging the single-pair images. LkH $\alpha$  198 was not bright enough for the observations to reach the diffraction limit, so the visibility was apodized to a cutoff frequency of 4 cycles arcsec $^{-1}$  and inverted to produce a final speckle image with 0".35 (FWHM) resolution.

## 3. RESULTS

The infrared images of the dark cloud containing LkH $\alpha$  198, shown in Figure 1, appear quite similar to the visible-light images published by a variety of workers. Both Ae/Be stars are surrounded by nebulosity with interesting non-circular structure, including an elliptical loop associated with LkH $\alpha$  198 and a sickle-shaped nebula near V376 Cas. These structures are seen most clearly in the shorter wavelength (1.25 and 1.65  $\mu\text{m}$ ) images. In order to bring out the structure of the extended emission close to LkH $\alpha$  198, images of the unresolved star HD 203856, which served as estimates of the PSF for the direct images, were subtracted. The HD 203856 images were scaled to the same peak values as LkH $\alpha$  198, and the HD 203856 and LkH $\alpha$  198 images were rebinned to a finer pixel grid to allow the peak of the HD 203856 images to be shifted to within  $\sim 0.2$  detector pixels (0".08) of the position of the LkH $\alpha$  198 peaks before subtracting. The resulting PSF-subtracted images of the region surrounding LkH $\alpha$  198 are shown in Figure 2. It is clear that the subtraction is imperfect within  $\sim 2''$  of the center, but it becomes reliable (and insensitive to the precise position of the PSF image) beyond that radius.

At the shortest wavelength, LkH $\alpha$  198 is seen to be surrounded by a fan-shaped nebula with an axis that lies close

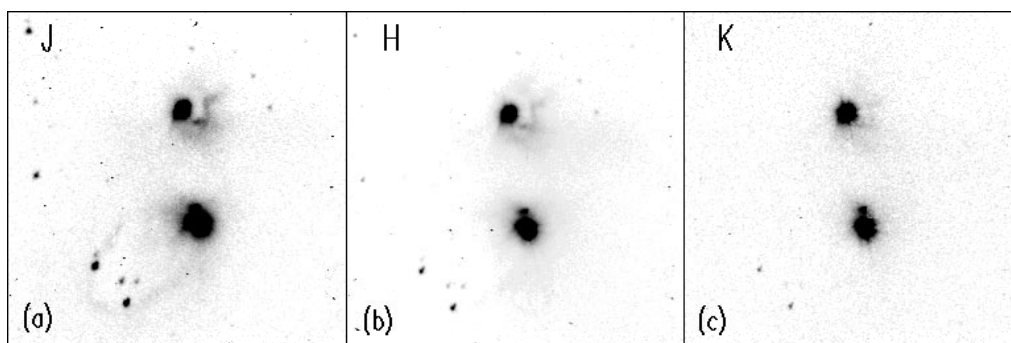


FIG. 1.— $J$  (1.25  $\mu\text{m}$ ),  $H$  (1.65  $\mu\text{m}$ ), and  $K$  (2.2  $\mu\text{m}$ ) band images of LkH $\alpha$  198 and V376 Cas (35" to the north) show the same basic structures seen in visible-light images by other workers. The extended emission at large distances from the stars tends to be brighter at the shorter wavelengths, as expected for scattering by small grains.

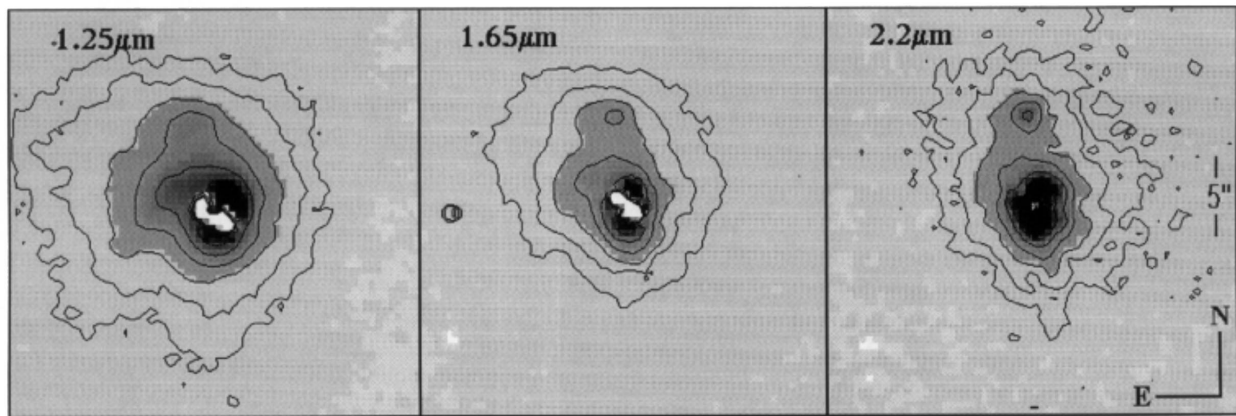


FIG. 2.—*J*, *H*, and *K* band images of LkH $\alpha$  198 formed by subtracting corresponding images of HD 203856 to bring out the extended structure. The contour levels are  $e^{-(1\dots6)}$  times the maximum value in each PSF-subtracted image.

to that of the elliptical loop that extends to the southeast. The PSF-subtracted infrared image reveals that the shape of the bright inner region of the nebula at scales smaller than the separation between LkH $\alpha$  198 and the IRC is similar to its shape at the larger ( $\sim 20''$ ) scales seen in visible-light images.

The appearance of the infrared companion, which was seen in mid-infrared images by Lagage et al. (1993)  $6''$  to the north of LkH $\alpha$  198, is nebulous at the shorter wavelengths but becomes more starlike at longer wavelengths. This can be seen more clearly in the cuts taken through the position of the IRC, presented in Figure 3.

The AOCSI image of LkH $\alpha$  198 is shown in Figure 4. Note that the lack of broad wings in the PSF permits the nebulosity to be studied significantly closer to the star despite the fact that the FWHM resolution of the image is not very much better than for the direct images. The dominant feature on scales of a few arcseconds is a barlike structure at PA  $\sim 20^\circ$ . This structure appears roughly symmetrical in extent about the central peak, but is brighter on its southern end. A blob  $\sim 5''$  north of the star is probably a weak detection of the infrared companion. Because that object fell on or close to the edge of the detector during the observations, it probably suffers strong distortions in both its appearance and its brightness.

The *H*-band speckle image of LkH $\alpha$  198 is presented in Figure 5. Despite having a significantly higher resolution than the AOCSI image ( $0''.35$  versus  $0''.8$  FWHM), the structure of the speckle image is roughly consistent with the AOCSI result, with the predominant feature being a barlike extension along PA  $\sim 30^\circ$ .

The radial dependence of the Fourier amplitude for LkH $\alpha$  198, computed by taking azimuthal averages of the two-dimensional amplitudes derived from the AOCSI and speckle observations, is shown in Figure 6. The amplitude curves are normalized to unity at zero frequency. They are consistent with each other through most of the measured frequency range. The amplitude derived from the speckle observations has smaller error bars and extends to higher frequency. It drops sharply with frequency and levels off at a value  $\sim 0.6$ , which represents an approximate measurement of the fraction of the total flux coming from an unresolved source.

Because of the novelty of the AOCSI technique and the desire to examine features at high resolution and sensi-

tivity, considerable care was taken to ensure that the uncertainties in the reconstructed images are well understood. Errors can come from detector noise and pickup and from variability of the optical transfer function. The former is straightforwardly estimated from the noise level in the image itself, but transfer function variability, which can

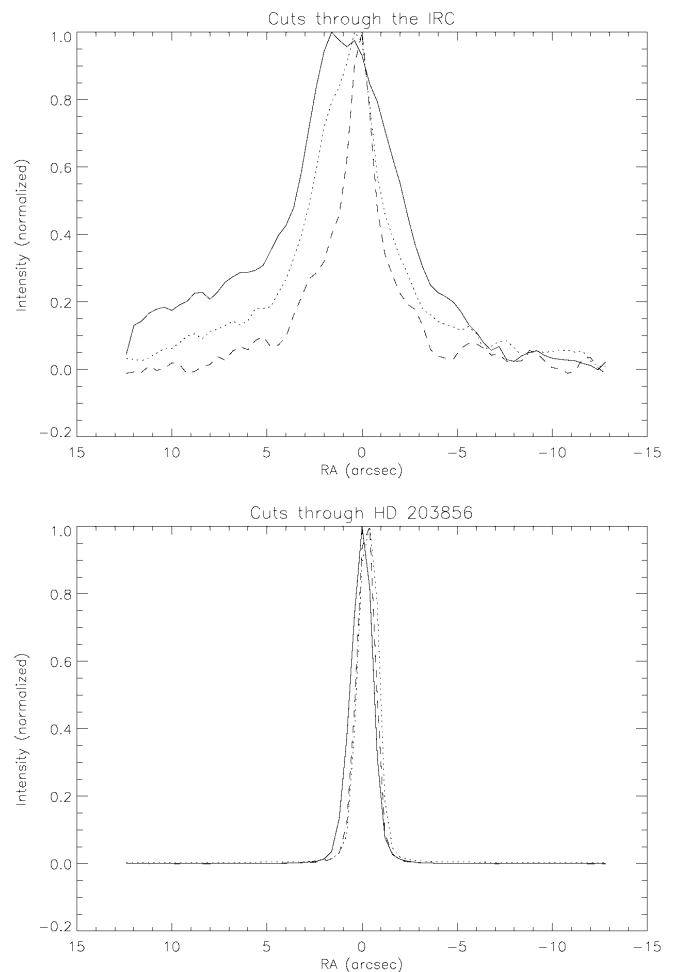


FIG. 3.—Profiles of the LkH $\alpha$  198 infrared companion formed by taking cuts through it in the east-west direction, together with cuts through the corresponding images of HD 203856. The  $1.25\ \mu\text{m}$  (solid),  $1.65\ \mu\text{m}$  (dotted), and  $2.2\ \mu\text{m}$  (dashed) curves clearly show the wavelength dependence of the size of the embedded object.

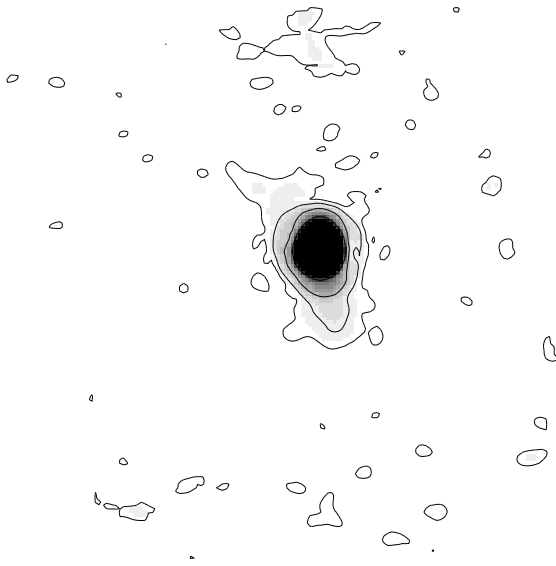


FIG. 4.—Image produced from the Starfire AOCSI data at  $H$ . Its size is  $181 \times 181$  pixels of  $0''.10$  each, so the total size of the image, including unsampled areas, is  $18'' \times 18''$ . Pixels are scaled linearly in intensity such that the peak of the image is saturated by a factor of 15. Contour levels are in steps of  $e^{-n}$  with  $n = 1 \dots 6$ . The apodization limit corresponds to a FWHM of  $0''.8$  for an unresolved source.

cause the final image to be over- or under-resolved or simply distorted, requires an examination of the impact of this variability on the reconstructed images. This is accomplished by reducing the LkH $\alpha$  198 data using only the reference-star series with the largest high-frequency power (to overresolve the object) and again using the reference

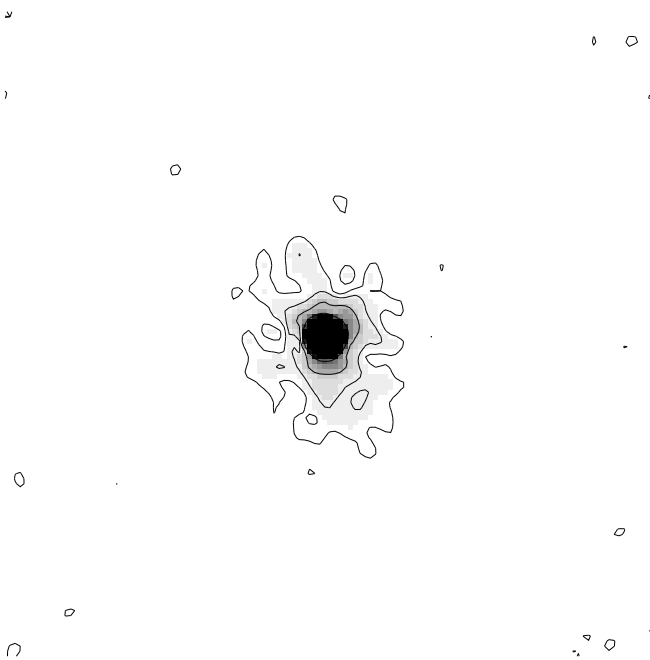


FIG. 5.—Image produced from the McDonald speckle data at  $H$ . Its size is  $128 \times 128$  pixels, corresponding to  $9'' \times 9''$ . Pixels are scaled linearly in intensity such that the peak of the image is saturated by a factor of 15. Contour levels are in steps of  $e^{-n}$  with  $n = 1 \dots 6$ . The apodization limit corresponds to 4 cycles  $\text{arcsec}^{-1}$  for the  $0''.07$  pixel size, or a FWHM of  $0''.35$ .

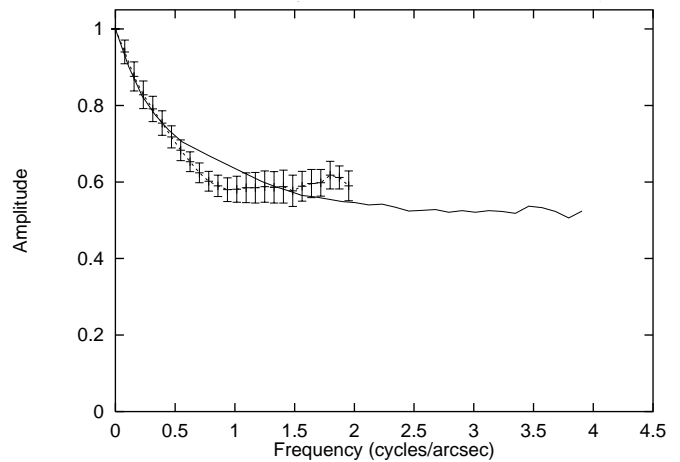


FIG. 6.—Azimuthally averaged Fourier amplitude curves from the AOCSI and speckle observations. The solid curve is based on the McDonald speckle data. Its uncertainties are smaller than those of the Starfire AOCSI data, which are shown as error bars.

series with the smallest high-frequency power. Aside from the expected difference in the breadth of the central peak, the structures in the resulting images were found to be reassuringly similar. Furthermore, the extended structures in the LkH $\alpha$  198 image are also seen at lower signal-to-noise in the reconstructions based on individual object + reference pairs. Together with the basic consistency between the AOCSI and speckle observations, which were made with different instruments on different telescopes, these tests inspire confidence that the basic results of these observations are reliable.

#### 4. DISCUSSION

The region surrounding LkH $\alpha$  198 is complex. The object appears nonstellar in visible and NIR images, with associated nebulosity some tens of arcseconds in extent. LkH $\alpha$  198 has an infrared companion  $\sim 6''$  to the north that is faint in visible and NIR images but becomes 40% as bright as the primary at  $12.3 \mu\text{m}$  (Lagage et al. 1993). In addition, Sandell & Weintraub (1994) report detection of a submillimeter protostar  $19''$  to the northwest of LkH $\alpha$  198. This object is the brightest submillimeter source in the region, but it has not been seen in infrared images. The positional relationships between the various features are illustrated in Figure 7.

LkH $\alpha$  198 and its infrared companion lie close to the apex of a fan-shaped nebula some  $20''$  across. The new PSF-subtracted NIR images reveal that the bright inner regions of the nebula are centered on the position of LkH $\alpha$  198, and that its shape on scales of a few arcseconds, smaller than the separation between LkH $\alpha$  198 and its infrared companion, is similar to the shape seen at larger scales in visible-light images. This suggests that the nebula is physically associated with LkH $\alpha$  198 and is not strongly influenced by the companion.

The fan-shaped nebula is located at the northwest end of a  $40''$  elliptical loop of reflection nebulosity that was first discovered by Bastien et al. (1988). One end of the loop traces the northwest side of the fan-shaped nebula. From there, the loop extends to the southeast along PA  $130^\circ$ . This



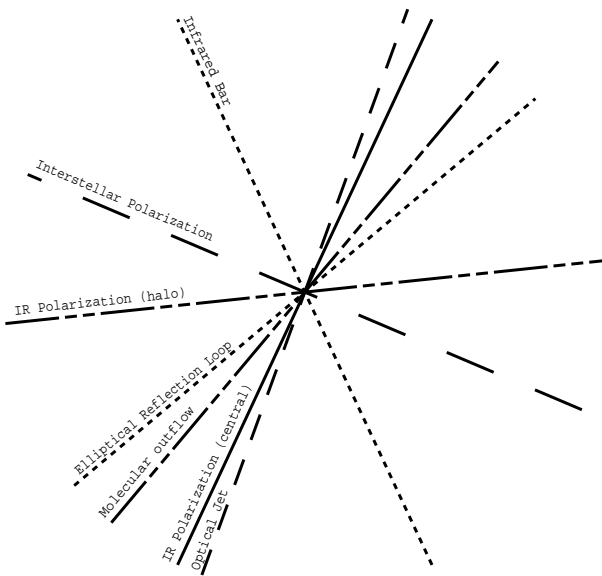


FIG. 8.—Position angles of various features associated with LkH $\alpha$  198 in graphical form. Note that the infrared polarization of the central object as measured by LHL at  $1.65 \mu\text{m}$  lies quite close to the position angle of the optical jet identified by CRB. This is consistent with a picture in which the polarization is produced by scattering of starlight from a flared circumstellar disk viewed nearly edge-on. The position angle of the infrared bar identified in the new AOCSI and speckle observations is approximately perpendicular to the polarization angle of the halo, as would be expected for starlight scattering in an optically thin medium.

collimated light emerging along the polar axis of a thick disk and scattering in an optically thin halo of ambient material. In that case, one would expect the bar's axis to be close to that of the optical jet.

A third possibility is that the bar represents light scattered within a “pseudodisk,” i.e., a disequilibrium disklike structure formed by the infall of cloud material along magnetic field lines with axial symmetry. The Lorentz force deflects infalling gas, which would otherwise flow along radial trajectories toward the protostar, so that it impacts the material flowing in the opposite direction at the equatorial plane (Galli & Shu 1993). These pseudodisks are distinct from, and typically an order of magnitude larger than, the classical optically thick, spatially thin, centrifugally supported circumstellar disks that are thought to exist around many pre-main sequence stars at scales of  $\sim 100$  AU. Because of ohmic dissipation and ambipolar diffusion, the magnetic forces are not strong enough to prevent the material within the pseudodisk from flowing inward, where it presumably feeds the true circumstellar disk.

Although they were calculated for a low-mass star, the isodensity contours for a model presented by Galli & Shu (1993) do qualitatively resemble the AOCSI and speckle images of LkH $\alpha$  198. Arguing against the pseudodisk model, however, is the fact that the orientation of the infrared bar is neither perpendicular to the interstellar magnetic field, as derived by LHL from polarization measurements of foreground and background stars, nor aligned with the inferred axis of the inner disk.

A final possibility, first raised by LHL to account for the polarization position angle of the halo at  $\sim 1''$  scales, is that the infrared bar is in some way associated with the sharp western edge of the fan-shaped reflection nebula. This sug-

gestion finds some support on geometrical grounds: the infrared bar is nearly perpendicular to the long axis of the elliptical reflection nebula and the molecular outflow (which we suggest above may be produced by the submillimeter protostar), and to that of the fan-shaped nebula seen in the  $1.25 \mu\text{m}$  image. The details of such a model remain unclear.

## 5. CONCLUSIONS

New NIR images of the young, nebulous intermediate-mass (Herbig Ae/Be) star LkH $\alpha$  198 using direct imaging, AOCSI, and standard speckle imaging reveal complex structure in its circumstellar dust distribution.

The new AOCSI and speckle observations have detected an infrared bar extending  $2''$ – $3''$  from the star in either direction. This bar is probably the source of the polarization of the LkH $\alpha$  198 system in the NIR at scales resolved by LHL's speckle polarimetry. The orientation of the bar with respect to this disk and to the interstellar magnetic field is not what would have been expected if the bar were the outer region of a standard circumstellar disk, a disequilibrium pseudodisk, or an ambient halo illuminated by starlight collimated by the circumstellar disk. Although the evidence is circumstantial at best, it appears more likely that the bar may be associated with the fan-shaped nebula seen in the  $1.25 \mu\text{m}$  infrared direct image, and possibly with the molecular outflow, to the axes of which the bar is roughly perpendicular.

The alignment of the polarization vector seen in the central point source by LHL with the position angle of the optical jet found by CRB makes it likely that LkH $\alpha$  198 is surrounded by a circumstellar disk, viewed nearly edge-on, which scatters much of the observable NIR starlight from its surface.

The infrared companion  $6''$  north of the star is seen to be significantly extended at NIR wavelengths, and its size decreases with wavelength. Its distance from LkH $\alpha$  198 and its surface brightness at  $1.25 \mu\text{m}$  appear consistent with its being seen primarily in reflected light at that wavelength. Polarization observations will be useful to confirm this model, and comparison of higher resolution observations with radiative-transfer calculations may provide interesting constraints on the structure of the envelope.

The relative proximity of the LkH $\alpha$  198 region has made it unusually amenable to study by a variety of techniques at high linear resolution and sensitivity. The many interrelated features that have been found surrounding this young intermediate-mass star make LkH $\alpha$  198 a good illustration of the complexity of the star formation process in nature and of the need for caution when one applies the necessarily simple theoretical models.

The McDonald observations and the construction of the D-LITE camera were supported by NASA grant NAGW-2323 and by a State of Texas ARP grant. The Starfire observations were made as part of a program sponsored by the NSF under grant AST 94-21225. A debt of gratitude is owed to the excellent staffs of the Starfire Optical Range and McDonald Observatory, without whose efforts these observations could not have been carried out, and to N. Evans for useful discussions. This research has made use of the Simbad database, operated at CDS, Strasbourg, France.

## REFERENCES

- Bastien, P., Ménard, F., Asselin, L., & Turbide, L. 1988, in *Modelling the Stellar Environment: How and Why?*, ed. P. Delache, S. Lalow, C. Magnan, & J. Tran Thanh Van (Paris: Editions Frontières), 85
- Cantó, J., Rodríguez, L. F., Calvet, N., & Levraut, R. M. 1984, *ApJ*, 282, 631
- Chavarría, K.-C. 1985, *A&A*, 148, 317
- Corcoran, D., Ray, T. P., & Bastien, P. 1995, *A&A*, 293, 550 (CRB)
- Di Francesco, J., Evans, N. J., II, Harvey, P. M., Mundy, L. G., & Butner, H. M. 1994, *ApJ*, 432, 710
- Fugate, R. Q., et al. 1994, *J. Opt. Soc. Am. A*, 11, 310
- Galli, D., & Shu, F. H. 1993, *ApJ*, 417, 243
- Herbig, G. 1960, *ApJS*, 4, 337
- Hillenbrand, L., Strom, S., Vrba, F., & Keene, J. 1992, *ApJ*, 397, 613
- Kataza, H., & Maihara, T. 1991, *A&A*, 248, L1
- Lagage, P. O., Olofsson, G., Cabrit, S., Cesarsky, C. J., Nordh, L., & Rodríguez Espinosa, J. M. 1993, *ApJ*, 427, L79
- Leinert, C., Haas, M., & Lenzen, R. 1991, *A&A*, 246, 180 (LHL)
- Leinert, C., Haas, M., & Weitzel, N. 1993, *A&A*, 271, 535
- Li, W., Evans, N. J., Harvey, P. M., & Colomé, C. 1994, *ApJ*, 433, 199
- Lohmann, A. W., Weigelt, G., & Wirnitzer, B. 1983, *Appl. Opt.*, 22, 4028
- Loren, R. B. 1977, *ApJ*, 218, 716
- Nakano, M., Kogure, T., Yoshida, S., & Tatematsu, K. 1990, *PASJ*, 42, 567
- Natta, A., Palla, F., Butner, H. M., Evans, N. J., II, & Harvey, P. M. 1993, *ApJ*, 406, 674
- Sandell, G., & Weintraub, D. A. 1994, *A&A*, 292, L1
- Strom, K., Strom, S., Wolff, S., Morgan, J., & Wenz, M. 1986, *ApJS*, 62, 39
- Whitney, B. A., & Hartmann, L. 1992, *ApJ*, 395, 529